J. Math. Anal. Appl. 346 (2008) 120–140

Contents lists available at ScienceDirect

J. Math. Anal. Appl.

www.elsevier.com/locate/jmaa

Central ADER schemes for hyperbolic conservation laws

Yousef Hashem Zahran

Physics and Mathematics Department, Faculty of Engineering, Port Said, Suez Canal University, Egypt

ARTICLE INFO

Article history:
Received 8 February 2008
Available online 16 May 2008
Submitted by J. Guermond

Keywords:
Hyperbolic conservation laws
ADER methods
WAF methods
TVD schemes
Upwind fluxes
Central fluxes
Convex flux
Non-convex flux
Burger equation
Euler equations

ABSTRACT

In this paper we first briefly review the very high order ADER methods for solving hyperbolic conservation laws. ADER methods use high order polynomial reconstruction of the solution and upwind fluxes as the building block. They use a first order upwind Godunov and the upwind second order weighted average (WAF) fluxes. As well known the upwind methods are more accurate than central schemes. However, the superior accuracy of the ADER upwind schemes comes at a cost, one must solve exactly or approximately the Riemann problems (RP). Conventional Riemann solvers are usually complex and are not available for many hyperbolic problems of practical interest. In this paper we propose to use two central fluxes, instead of upwind fluxes, as the building block in ADER scheme. These are the monotone first order Lax–Friedrich (LXF) and the third order TVD flux. The resulting schemes are called central ADER schemes. Accuracy of the new schemes is established. Numerical implementations of the new schemes are carried out on the scalar conservation laws with a linear flux, nonlinear convex flux and non-convex flux. The results demonstrate that the proposed scheme, with LXF flux, is comparable to those using first and second order upwind fluxes while the scheme, with third order TVD flux, is superior to those using upwind fluxes. When compared with the state of art ADER schemes, our central ADER schemes are faster, more accurate, Riemann solver free, very simple to implement and need less computer memory. A way to extend these schemes to general systems of nonlinear hyperbolic conservation laws in one and two dimensions is presented.

1. Introduction

Hyperbolic conservation laws arise in areas as diverse as compressible gas dynamics, shallow water flow, weather prediction, plasma modelling, rarefied gas dynamics and many others. Analytical solutions are available only in very few special case and numerical methods must be used in practical applications. It is well known that the solutions of hyperbolic equations laws may develop discontinuities in finite time even when the initial condition is smooth. A successful method should compute such discontinuities with the correct position and without spurious oscillations and retain high order of accuracy in smooth regions.

As is well known from the theorem of Godunov [9,11,16], high order linear schemes will generate spurious oscillations near discontinuities or sharp gradients of the solution. These oscillations pollute the numerical solution and are thus highly undesirable. To avoid generating spurious oscillations, nonlinear solution-adaptive schemes must be constructed. Over the last thirty years or so much work has been done to circumvent Godunov theorem, which involves the design of schemes that must necessarily be nonlinear, even if applied to linear problems. Amongst successful development in this direction we have TVD methods [2], ENO [3] and WENO methods [1,4] and more recently, ADER methods [8–17].

E-mail address: yousef_hashem_zahran@yahoo.com.

0022-247X/$ – see front matter
doi:10.1016/j.jmaa.2008.05.032

TVD schemes are second order (or higher) accurate and avoid oscillations by locally reverting to first order accuracy near discontinuities and extrema. Therefore TVD schemes are unsuitable for special applications areas such as acoustics, compressible turbulence and problems involving long time evolution wave propagation. In these applications extrema are clipped as time evolves and numerical dissipation may become dominant.

Uniformly very high order methods, in time and space, are needed for such applications. Examples include the class of essentially non-oscillatory (ENO), weighted essentially non-oscillatory WENO schemes and ADER methods. ENO and WENO schemes are essentially non-oscillatory. That is, to the eye, the solution is free from spurious oscillations and such oscillations can be shown to decay as the mesh is refined.

ADER approach is recently developed as a generalisation of the upwind Godunov's method and rely on the solution of a generalised Riemann problem (GRP) with initial condition consisting of polynomial functions of arbitrary order. The solution of this difficult problem is reduced to the solution of a sequence of m conventional Riemann problems (RP). For nonlinear problems the first of these is a nonlinear RP and the remaining ones are linear RPs for the kth order spatial derivatives of the initial conditions, with $k = 0, 1, \ldots, m-1$, where m is arbitrary and is the order of accuracy of the resulting scheme. The ADER schemes are conservative, one step, explicit and fully discrete, requiring only the computation of the intercell flux to advance the solution by a full time step. To evaluate the numerical flux, in the ADER schemes, one solves the generalised RP, exactly or numerically with initial condition consisting of two arbitrary but smooth functions using a semi-analytical method. To avoid the Gibbs phenomenon the ADER approach relies on WENO reconstructions of the data from cell averages. However, the superior accuracy of the ADER upwind schemes comes at a cost, one must solve exactly or approximately, the RP. Conventional Riemann solvers are usually complex and are not available for many hyperbolic systems of practical interest. It is thus desirable to construct a numerical flux that emulates the upwind best flux available (ADER) with the simplicity and generality of central fluxes.

In [8,12,16] Toro and Takakura presented a new version of ADER approach in which the Taylor expansion is performed in terms of the flux function. They built the flux rather than the state expansion in time to achieve an arbitrary order of accuracy in space and time. Also, Titarev and Toro [12,16] and Takakura [8] proposed to use the second order upwind TVD weighted average flux (WAF) [13] flux, instead of first order upwind Godunov flux as the building block. The scheme is called ADER-WAF scheme.

The main motivation of this paper is to enhance the accuracy and simplicity of the ADER schemes by making use of the central fluxes as part of the flux expansion of the solution of the GRP. In this paper we propose to use central flux, instead of upwind fluxes, as the building block. We call the new improved schemes CENTRAL-ADER schemes. There appear to be two candidate fluxes that can be readily used as the building block. These are the first order monotone Lax–Friedrich (LXF) flux and the third order TVD flux [19]. Both fluxes are central and therefore avoid the solution of the RPs. When compared with the state of art ADER schemes, our central schemes are faster, more accurate, Riemann solver free, very simple to implement and need less computer memory. We carry out a systematic assessment of the constructed numerical schemes. We do so for a set of carefully selected test problems, with particular emphasis on testing the accuracy of the schemes for very long time evolution, as it is long time evolution for which the sophistication high order must be justified and for the problems of complicated wave formation and interaction in the nonlinear cases corresponding to convex and non-convex fluxes. We compare the results against exact solutions. The new schemes are systematically compared with ADER-WAF and original ADER schemes.

The rest of the paper is organised as follows. In Section 2 we review the original ADER methods. The central ADER scheme with first order flux is described in Section 3. In Section 4 we introduce the central ADER scheme with third order TVD flux. Accuracy of the new schemes is discussed in Section 5. Numerical results are given in Section 6. Extension of the schemes for systems equations in one dimension is presented in Section 7. Finally the extension in two dimension is described in Section 8.

2. ADER approach

In this section the ADER approach is reviewed for the following hyperbolic conservation law

$$u_t + f(u)_x = 0, \quad -\infty < x < \infty, \ t \geqslant 0, \tag{2.1a}$$

along with the initial condition

$$u(x,0) = u_0(x) \tag{2.1b}$$

Eqs. (2.1) may be written in the form

$$u_t + \lambda(u) u_x = 0, \tag{2.2}$$

where $\lambda(u)$ is the characteristic speed defined by $\lambda(u) = \frac{df}{du}$. Integration of (2.1) over the control volume in x–t space $[x_{j-\frac{1}{2}}, x_{j+\frac{1}{2}}] \times [t^n, t^{n+1}]$, of dimensions $\Delta x = x_{j+\frac{1}{2}} - x_{j-\frac{1}{2}}$, $\Delta t = t^{n+1} - t^n$ we obtain

$$u_j^{n+1} = u_j^n - \frac{\Delta t}{\Delta x}\left[F_{j+\frac{1}{2}} - F_{j-\frac{1}{2}}\right], \tag{2.3}$$

where u_j^n is the space average of the solution in the cell $I_j = [x_{j-\frac{1}{2}}, x_{j+\frac{1}{2}}]$ at t^n and the flux $F_{j+\frac{1}{2}}$ is the time average of the physical flux at the cell interface $x_{j+\frac{1}{2}}$:

$$u_j^n = \frac{1}{\Delta x}\int_{x_{j-\frac{1}{2}}}^{x_{j+\frac{1}{2}}} u(x,t^n)\,dx, \qquad F_{j+\frac{1}{2}} = \frac{1}{\Delta t}\int_{t^n}^{t^{n+1}} f\big(u(x_{j+\frac{1}{2}})\big)\,dt. \tag{2.4}$$

The description of the scheme is complete when a proper non-oscillatory flux is chosen.

The ADER approach defines numerical fluxes in such a way that the explicit conservative one step formula (2.3) computes numerical solutions of (2.1) to arbitrary high order of accuracy in both space and time.

The ADER approach in state series expansion consists of the following steps:

(i) *Reconstruction*. To avoid spurious oscillations ENO or WENO reconstruction can be used. In general, WENO reconstruction produces more accurate results and therefore it is used in design of our schemes. By means of the reconstruction step the conservative variable is represented by polynomials $P_j(x)$ in each cell I_j. At each cell interface $x_{j+\frac{1}{2}}$ we then have the following GRP:

$$\left.\begin{aligned} &u_t + f(u)_x = 0,\\ &u(x,0) = \begin{cases} u_L(x) = P_j, & x < x_{j+\frac{1}{2}}\\ u_R(x) = P_{j+1}, & x > x_{j+\frac{1}{2}} \end{cases} \end{aligned}\right\}. \tag{2.5}$$

We remark that for the mth order accurate scheme the reconstruction polynomials must be of $(m-1)$th order. In all numerical examples given here we use the 5th order WENO reconstruction [1,4].

(ii) *State expansion*. We find an approximate solution for the interface state $u(x_{j+\frac{1}{2}}, \tau)$, where τ is local time $\tau = t - t^n$ assumed to be sufficiently small. First we write a Taylor expansion of the interface state in time:

$$u(x_{j+\frac{1}{2}}, \tau) = u(x_{j+\frac{1}{2}}, 0+) + \sum_{k=1}^{m-1}\left\{\frac{\partial^k}{\partial t^k}u(x_{j+\frac{1}{2}}, 0+)\right\}\frac{\tau^k}{k!}, \tag{2.6}$$

where $0+ = \lim_{t\to 0+} t$. If Eq. (2.2) is linear with constant speed λ, time derivatives are

$$\frac{\partial^k u}{\partial t^k} = (-\lambda)^k \frac{\partial^k u}{\partial x^k}. \tag{2.7}$$

When Eq. (2.2) is nonlinear, the Cauchy–Kowalewski (see [8]) procedure is then applied to replace all time derivatives in expansion by space derivatives as follows:

$$\begin{aligned}
&u_t^{(1)} = -\lambda u_x^{(1)}, \qquad u_t^{(2)} = \lambda^2 u_x^{(2)} + 2\lambda\lambda_u\big(u_x^{(1)}\big)^2,\\
&u_t^{(3)} = -\lambda^3 u_x^{(3)} - 9\lambda^2\lambda_u u_x^{(1)} u_x^{(2)} - 6\lambda(\lambda_u)^2\big(u_x^{(1)}\big)^3 - 3\lambda^2\lambda_{uu}\big(u_x^{(1)}\big)^3,\\
&u_t^{(4)} = \lambda^4 u_x^{(4)} + 16\lambda^3\lambda_u u_x^{(1)} u_x^{(3)} + 12\lambda^3\lambda_u\big(u_x^{(2)}\big)^2 + 72\lambda^2\big(\lambda_u\big)^2\big(u_x^{(1)}\big)^2 u_x^{(2)}\\
&\qquad + 24\lambda(\lambda_u)^3\big(u_x^{(1)}\big)^4 + 24\lambda^3\lambda_{uu}\big(u_x^{(1)}\big)^2 u_x^{(2)} + 36\lambda^2\lambda_u\lambda_{uu}\big(u_x^{(1)}\big)^4 + 4\lambda^3\lambda_{uuu}\big(u_x^{(1)}\big)^4,\\
&u_t^{(k)} = A^{(k)}\big(u_x^{(0)}, u_x^{(1)}, \ldots, u_x^{(k)}\big).
\end{aligned} \tag{2.8}$$

Therefore, the time Taylor series expansion becomes

$$u(x_{j+\frac{1}{2}}, \tau) = u(x_{j+\frac{1}{2}}, 0+) + \sum_{k=1}^{m-1}\big\{A^{(k)}\big(u_x^{(0)}(x_{j+\frac{1}{2}}, 0+), \ldots, u_x^{(k)}(x_{j+\frac{1}{2}}, 0+)\big)\big\}\frac{\tau^k}{k!}. \tag{2.9}$$

The leading term $u(x_{j+\frac{1}{2}}, 0+)$ accounts for the first instant interaction of the boundary extrapolated values $u_L(x_{j+\frac{1}{2}}, 0)$ and $u_R(x_{j+\frac{1}{2}}, 0)$. This leading term is computed by solving the conventional (piece wise constant) RP:

$$\left.\begin{aligned} &u_t + f(u)_x = 0,\\ &u(x,0) = \begin{cases} u_L(x_{j+\frac{1}{2}}), & x < x_{j+\frac{1}{2}}\\ u_R(x_{j+\frac{1}{2}}), & x > x_{j+\frac{1}{2}} \end{cases} \end{aligned}\right\} \tag{2.10}$$

by using the upwind Godunov method. The remaining terms $u_x^{(k)}(x_{j+\frac{1}{2}}, 0+)$ $(k = 1, 2, \ldots, m-1)$ are the solutions of the kth order derivative RP locally linearised around the leading term $u_x^{(0)}(x_{j+\frac{1}{2}}, 0+)$ of (2.9):

$$\left.\begin{aligned} &v_t + \lambda\big(u(x_{j+\frac{1}{2}}, 0+)\big)v_x = 0, \\ &v(x,0) = \begin{cases} u_L^{(k)}(x_{j+\frac{1}{2}}), & x < x_{j+\frac{1}{2}} \\ u_R^{(k)}(x_{j+\frac{1}{2}}), & x > x_{j+\frac{1}{2}} \end{cases} \end{aligned}\right\}, \tag{2.11}$$

where $v = u_x^{(k)}$ and they are given as Godunov state. Finally, having all spatial terms we form the Taylor expansion (2.9). The numerical flux is evaluated by using an appropriate mth order accurate Gaussian rule

$$F_{j+\frac{1}{2}} = \sum_{\alpha=0}^{N} F\big(u(x_{j+\frac{1}{2}}, \gamma_\alpha \Delta t)\big) K_\alpha, \tag{2.12}$$

where γ_j and K_j are properly scaled nodes and weights of the rule and N is the number of nodes [8,16].

A key ingredient here is the availability of an exact or approximate solver to provide the terms of (2.9).

3. Central ADER approach

Now, we propose to use central fluxes, instead of upwind fluxes, as building block. We call the new scheme CENTRAL-ADER scheme. There appear to be two candidate fluxes that can be used as the building blocks. These are the monotone first order LXF flux and the third order TVD flux [19].

3.1. ADER method with first order central fluxes

To compute the terms of (2.9) we proceed as follows:

The leading term of (2.9) should be computed by a monotone method, to avoid entropy violation. Probably the most well-known centered monotone method is the Lax–Friedrich method.

The leading term $u(x_{j+\frac{1}{2}}, 0+)$ accounts for the first instant interaction of the boundary extrapolated values $u_L(x_{j+\frac{1}{2}}, 0)$ and $u_R(x_{j+\frac{1}{2}}, 0)$ and it is the solution the conventional (piece wise constant) RP:

$$\left.\begin{aligned} &u_t + f(u)_x = 0, \\ &u(x,0) = \begin{cases} u_L(x_{j+\frac{1}{2}}), & x < x_{j+\frac{1}{2}} \\ u_R(x_{j+\frac{1}{2}}), & x > x_{j+\frac{1}{2}} \end{cases} \end{aligned}\right\}. \tag{3.1}$$

Here we use the staggered form of LXF scheme [5] of Eq. (3.1)

$$u_{j+\frac{1}{2}}^{0+} = \frac{1}{2}\big[u_L(x_{j+\frac{1}{2}}, 0) + u_R(x_{j+\frac{1}{2}}, 0)\big] - \frac{\alpha_0 \Delta t}{\Delta x}\big[f\big(u_R(x_{j+\frac{1}{2}}, 0)\big) - f\big(u_L(x_{j+\frac{1}{2}}, 0)\big)\big]. \tag{3.2}$$

In the limiting case of piece wise constant data $u_L(x_{j+\frac{1}{2}}) = u_j^n$ and $u_R(x_{j+\frac{1}{2}}) = u_{j+1}^n$ this scheme leads to a monotone first order LXF in staggered form [5]

$$u_{j+\frac{1}{2}}^{0+} = \frac{1}{2}\big[u_j^0 + u_{j+1}^0\big] - \frac{\alpha_0 \Delta t}{\Delta x}\big[f\big(u_{j+1}^0\big) - f\big(u_j^0\big)\big]. \tag{3.3}$$

Expression (3.2) is a generalised of (3.3) to higher order reconstructions. $u_x^{(k)}(x_{j+\frac{1}{2}}, 0+)$ $(k = 1, 2, \ldots, m-1)$ are the solutions of the kth order derivative RP (2.11) locally linearised around the leading term $u(x_{j+\frac{1}{2}}, 0+)$ of (3.3) and they are computed by staggered LXF scheme:

$$v_{j+\frac{1}{2}}^{0+} = \frac{1}{2}\big[v_L(x_{j+\frac{1}{2}}, 0) + v_R(x_{j+\frac{1}{2}}, 0)\big] - \lambda \frac{\alpha_k \Delta t}{\Delta x}\big[v_R(x_{j+\frac{1}{2}}, 0) - v_L(x_{j+\frac{1}{2}}, 0)\big]. \tag{3.4}$$

Here the time weight $\alpha_k = \frac{1}{(k+1)^{\frac{1}{k}}}$, $k \geqslant 1$, see [14]. It is easy to see that α_k lie in the interval $[0.5, 1]$ and we take $\alpha_0 = 0.36788$.

In the limiting case this scheme leads to a monotone first order LXF in staggered form

$$v_{j+\frac{1}{2}}^{0+} = \frac{1}{2}\big[v_j^0 + v_{j+1}^0\big] - \lambda \frac{\alpha_k \Delta t}{\Delta x}\big[v_{j+1}^0 - v_j^0\big]. \tag{3.5}$$

Having obtained all spatial derivatives we form the Taylor expansion (2.9). Two options exist to evaluate the numerical flux $F_{j+\frac{1}{2}}$ of Eq. (2.3). The first one is state expansion ADER [8,11,13], in which an appropriate mth order accurate Gaussian rule is used to evaluate the numerical flux

$$F_{j+\frac{1}{2}} = \sum_{\alpha=0}^{N} F\big(u(x_{j+\frac{1}{2}}, \gamma_\alpha \Delta t)\big) K_\alpha, \tag{3.6}$$

where γ_j and K_j are properly scaled nodes and weights of the rule and N is the number of nodes. When $F_{j+\frac{1}{2}}$ is used with the conservative form (2.3), the mth order ADER state series expansion is obtained.

The second option will be discussed in the next section.

3.1.1. Flux expansion

The idea of the flux expansion is to use the Taylor expansion of the flux directly, instead of using the Gaussian procedure (3.6). Firstly, by multiplying (2.1) by $\lambda(u)$ we get the conservative law for the flux f:

$$f_t + \lambda(u) f_x = 0. \tag{3.7}$$

At $t = t^n$ we reconstruct the fluxes to piece-wise smooth functions $g_j(x) = f(P_j(x))$, then near each cell interface $x_{j+\frac{1}{2}}$ we consider the following GRP:

$$\left.\begin{aligned} &f_t + \lambda(u) f_x = 0, \\ &f(x,0) = \begin{cases} g_j(x_{j+\frac{1}{2}}), & x < x_{j+\frac{1}{2}} \\ g_{j+1}(x_{j+\frac{1}{2}}), & x > x_{j+\frac{1}{2}} \end{cases} \end{aligned}\right\}. \tag{3.8}$$

We seek Taylor time expansion of the physical flux at $x_{j+\frac{1}{2}}$:

$$f(x_{j+\frac{1}{2}}, \tau) = f(x_{j+\frac{1}{2}}, 0+) + \sum_{k=1}^{m-1} \left\{ \frac{\partial^k}{\partial t^k} f(x_{j+\frac{1}{2}}, 0+) \right\} \frac{\tau^k}{k!}. \tag{3.9}$$

For linear case, i.e., λ is constant, all derivatives can be replaced with space derivatives of f:

$$\frac{\partial^k f}{\partial t^k} = (-\lambda)^k \frac{\partial^k f}{\partial x^k}. \tag{3.10}$$

When Eq. (2.2) is nonlinear, the Cauchy–Kowalewski (see [7]) procedure is then applied to replace all time derivatives in expansion by space derivatives as follows:

$$\begin{aligned} &f_t^{(1)} = -\lambda f_x^{(1)}, \qquad f_t^{(2)} = \lambda^2 f_x^{(2)} + 2\lambda_u \big(f_x^{(1)}\big)^2, \\ &f_t^{(3)} = -\lambda^3 f_x^{(3)} - 9\lambda\lambda_u f_x^{(1)} f_x^{(2)} - \frac{3}{\lambda}(\lambda_u)^2 \big(f_x^{(1)}\big)^3 - 3\lambda_{uu}\big(f_x^{(1)}\big)^3, \\ &f_t^{(4)} = \lambda^4 f_x^{(4)} + 16\lambda^2\lambda_u f_x^{(1)} f_x^{(3)} + 12\lambda^2\lambda_u \big(f_x^{(2)}\big)^2 + 48(\lambda_u)^2 \big(f_x^{(1)}\big)^2 f_x^{(2)} \\ &\qquad + 24\lambda\lambda_{uu}\big(f_x^{(1)}\big)^2 f_x^{(2)} + \frac{20}{\lambda}\lambda_u\lambda_{uu}\big(f_x^{(1)}\big)^4 + 4\lambda_{uuu}\big(f_x^{(1)}\big)^4, \\ &f_t^{(k)} = B^{(k)}\big(f_x^{(0)}, f_x^{(1)}, \ldots, f_x^{(k)}\big). \end{aligned} \tag{3.11}$$

Therefore, the time Taylor series expansion becomes

$$f(x_{j+\frac{1}{2}}, \tau) = f(x_{j+\frac{1}{2}}, 0+) + \sum_{k=1}^{m-1} \big\{ B^{(k)}\big(f_x^{(0)}(x_{j+\frac{1}{2}}, 0+), \ldots, f_x^{(k)}(x_{j+\frac{1}{2}}, 0+)\big) \big\} \frac{\tau^k}{k!}. \tag{3.12}$$

The leading term $f(x_{j+\frac{1}{2}}, 0+)$ is computed as flux of Eq. (2.10):

$$f(x_{j+\frac{1}{2}}, 0+) = f\big(u(x_{j+\frac{1}{2}}, 0+)\big), \tag{3.13}$$

where $u(x_{j+\frac{1}{2}}, 0+)$ is given in (3.3). $f_x^{(k)}(x_{j+\frac{1}{2}}, 0+)$ $(k = 1, 2, \ldots, m-1)$ are the solutions of the kth order derivative RP locally linearised around the leading term $u(x_{j+\frac{1}{2}}, 0+)$:

$$\left.\begin{aligned} &w_t + \lambda\big(u(x_{j+\frac{1}{2}}, 0+)\big) w_x = 0, \\ &w(x,0) = \begin{cases} f_L^{(k)}(x_{j+\frac{1}{2}}), & x < x_{j+\frac{1}{2}} \\ f_R^{(k)}(x_{j+\frac{1}{2}}), & x > x_{j+\frac{1}{2}} \end{cases} \end{aligned}\right\}, \tag{3.14}$$

where $w = f_x^{(k)}$ and $f_L^{(k)}(x_{j+\frac{1}{2}}, 0+) = \lim_{x\to x_{j+\frac{1}{2}}^{-0}} \partial_x^{(k)} g_j$, $f_R^{(k)}(x_{j+\frac{1}{2}}, 0+) = \lim_{x\to x_{j+\frac{1}{2}}^{+0}} \partial_x^{(k)} g_{j+1}$ and they are given by staggered LXF method (see [5]):

$$w_{j+\frac{1}{2}}^{0+} = f_{j+\frac{1}{2}}^{(k)0+} = \frac{1}{2}\big[w_j^0 + w_{j+1}^0\big] - \lambda\frac{\alpha_k \Delta t}{\Delta x}\big[w_{j+1}^0 - w_j^0\big]. \tag{3.15}$$

The mth order ADER numerical flux is given by time average

$$F_{j+\frac{1}{2}} = \frac{1}{\Delta t}\int_0^{\Delta t} f\big(u(x_{j+\frac{1}{2}}, \tau)\big)\,d\tau = f(x_{j+\frac{1}{2}}, 0+) + \sum_{k=1}^{m-1}\big\{B^{(k)}\big(f_x^{(0)}(x_{j+\frac{1}{2}}, 0+), \ldots, f_x^{(k)}(x_{j+\frac{1}{2}}, 0+)\big)\big\}\frac{(\Delta t)^k}{(k+1)!}. \tag{3.16}$$

Substituting of the flux (3.16) into (2.3) gives the sought solution at time t^{n+1} and the full scheme may be written as:

$$u_j^{n+1} = u_j^n - \frac{(\Delta t)_0}{\Delta x}\big\{f_{j+\frac{1}{2}}^{(0)} - f_{j-\frac{1}{2}}^{(0)}\big\} - \sum_{k=1}^{m-1}\big\{B_{j+\frac{1}{2}}^{(k)} - B_{j-\frac{1}{2}}^{(k)}\big\}\frac{(\Delta t)_k}{\Delta x} \tag{3.17}$$

with $(\Delta t)_k = \frac{(\Delta t)^{k+1}}{(k+1)!}$ and $f_{j+\frac{1}{2}}^{(0)} = f(u(x_{j+\frac{1}{2}}, 0+))$.

Then Eq. (3.17) can be interpreted as summation of the solutions evolutional equations of state variable $u = \partial_x^{(0)} u$ (first line) and its gradients $\partial_x^{(k)} u$ (second line) by LXF first order central scheme.

This leads to the idea to replace the LXF scheme by the third order TVD scheme [19] in all terms in the Taylor expansion.

4. ADER method with third order TVD flux

The main motivation of this paper is to enhance the accuracy and simplicity of the ADER schemes by making use of the central third order TVD flux [19] as part of the flux expansion of the solution of GRP (2.5). That is, we propose to use a central third order TVD flux rather than a first order flux as the building block of our high order methods.

In the next section we firstly briefly review the third order TVD flux [19] which will be incorporated in the framework ADER schemes.

4.1. Third order TVD scheme

In this section the third order TVD scheme presented in [19] is reviewed.

First let us consider the linear case, i.e., λ is a constant wave speed.

The conservative third order TVD numerical fluxes introduced in [18] has the form:

$$f_{j+\frac{1}{2}} = \frac{1}{2}(\lambda u_j + \lambda u_{j+1}) - \frac{1}{2}|\lambda|\Delta_{j+\frac{1}{2}} u + |\lambda|\{A_0\Delta_{j+\frac{1}{2}} u + A_1\Delta_{j+L+\frac{1}{2}} u\}\phi_j + |\lambda|A_2\Delta_{j+M+\frac{1}{2}} u\phi_{j+M}, \tag{4.1}$$

where $L = -1$, $M = 1$ for $c > 0$ and $L = 1$, $M = -1$ for $c < 0$.

Here $c = \lambda\frac{\Delta t}{\Delta x}$ is the Courant number and $\Delta_{j+\frac{1}{2}} u = u_{j+1} - u_j$ and

$$A_0 = \frac{1}{2} - \frac{|c|}{4}, \qquad A_1 = -\frac{|c|}{8} - \frac{c^2}{8}, \qquad A_2 = -\frac{|c|}{8} + \frac{c^2}{8}. \tag{4.2}$$

Here ϕ_j and ϕ_{j+M} are flux limiter functions see [7] and [19].

For nonlinear scalar problems $\lambda = \lambda(u)$, we define the wave speed

$$\lambda_{j+\frac{1}{2}} = \begin{cases} \frac{\Delta_{j+\frac{1}{2}} f}{\Delta_{j+\frac{1}{2}} u}, & \Delta_{j+\frac{1}{2}} u \neq 0, \\ \frac{\partial f}{\partial u}\big|_{u_j}, & \Delta_{j+\frac{1}{2}} u = 0. \end{cases} \tag{4.3}$$

The numerical flux (4.2) takes the form

$$f_{j+\frac{1}{2}} = \frac{1}{2}(f_j + f_{j+1}) - \frac{1}{2}|\lambda_{j+\frac{1}{2}}|\Delta_{j+\frac{1}{2}} u + |\lambda_{j+\frac{1}{2}}|\{A_0\Delta_{j+\frac{1}{2}} u + A_1\Delta_{j+L+\frac{1}{2}} u\}\phi_j + |\lambda_{j+\frac{1}{2}}|A_2\Delta_{j+M+\frac{1}{2}} u\phi_{j+M}. \tag{4.4}$$

The coefficients A_j are the same (4.2) with replacing c by $c_{j+\frac{1}{2}} = \frac{\Delta t}{\Delta x}\lambda_{j+\frac{1}{2}}$.

The stability condition for the above schemes is

$$\mathrm{CFL} \leqslant 1, \tag{4.5}$$

where $\mathrm{CFL} = \max_j(S_j^n\frac{\Delta t}{\Delta x})$. Here S_j^n is the maximum propagation speed in I_j at time level n.

4.2. Central ADER with third order flux

The scheme depends on the Taylor series expansion directly for flux n by Eq. (3.12).

The leading term $f(x_{j+\frac{1}{2}}, 0+)$ is computed as flux of equation

$$\left.\begin{aligned} &u_t + f(u)_x = 0, \\ &u(x,0) = \begin{cases} u_L(x_{j+\frac{1}{2}}), & x < x_{j+\frac{1}{2}} \\ u_R(x_{j+\frac{1}{2}}), & x > x_{j+\frac{1}{2}} \end{cases} \end{aligned}\right\}. \tag{4.6}$$

Here we use the two step method in which the first step is the non-staggered LXF method and the second step is the third order TVD flux:

$$\begin{aligned} &\text{(i)} \quad u_j^{0+} = \frac{1}{2}\big[u_{j+1}^0 + u_{j-1}^0\big] - \frac{\alpha_k \Delta t}{2\Delta x}\big[f_{j+1}^0 - f_{j-1}^0\big], \\ &\text{(ii)} \quad f_{j+\frac{1}{2}}^{0+} = \frac{1}{2}\big(f_j^{0+} + f_{j+1}^{0+}\big) - \frac{1}{2}|\lambda_{j+\frac{1}{2}}|\Delta_{j+\frac{1}{2}} u^{0+} + |\lambda_{j+\frac{1}{2}}|\big\{A_0 \Delta_{j+\frac{1}{2}} u^{0+} + A_1 \Delta_{j+L+\frac{1}{2}} u^{0+}\big\}\phi_j \\ &\qquad\qquad + |\lambda_{j+\frac{1}{2}}| A_2 \Delta_{j+M+\frac{1}{2}} u^{0+} \phi_{j+M}, \end{aligned} \tag{4.7}$$

$f_x^{(k)}(x_{j+\frac{1}{2}}, 0+)$ $(k = 1, 2, \ldots, m-1)$ are computed as fluxes of the kth order RP on f locally linearised:

$$\left.\begin{aligned} &w_t + \lambda\big(u(x_{j+\frac{1}{2}}, 0+)\big) w_x = 0, \\ &w(x,0) = \begin{cases} u_L^{(k)}(x_{j+\frac{1}{2}}), & x < x_{j+\frac{1}{2}} \\ u_R^{(k)}(x_{j+\frac{1}{2}}), & x > x_{j+\frac{1}{2}} \end{cases} \end{aligned}\right\}, \tag{4.8}$$

where $w = u_x^{(k)}$.

They are given by the two step method:

$$\begin{aligned} &\text{(i)} \quad w_j^{0+} = \frac{1}{2}\big[w_{j+1}^0 + w_{j-1}^0\big] - \frac{\alpha_k \Delta t}{2\Delta x}\big[f_{j+1}^0 - f_{j-1}^0\big], \\ &\text{(ii)} \quad f_{j+\frac{1}{2}}^{0+} = \frac{1}{2}\big(f_j^{0+} + f_{j+1}^{0+}\big) - \frac{1}{2}|\lambda_{j+\frac{1}{2}}|\Delta_{j+\frac{1}{2}} w^{0+} + |\lambda_{j+\frac{1}{2}}|\big\{A_0 \Delta_{j+\frac{1}{2}} w^{0+} + A_1 \Delta_{j+L+\frac{1}{2}} w^{0+}\big\}\phi_j \\ &\qquad\qquad + |\lambda_{j+\frac{1}{2}}| A_2 \Delta_{j+M+\frac{1}{2}} w^{0+} \phi_{j+M}, \end{aligned} \tag{4.9}$$

where $f_j = \lambda w_j$. Substituting of the flux (4.9) into (2.3) gives the sought solution at time t^{n+1} and the full scheme may be written as:

$$u_j^{n+1} = u_j^n - \frac{(\Delta t)_k}{\Delta x}\big\{f_{j+\frac{1}{2}}^{(0)} - f_{j-\frac{1}{2}}^{(0)}\big\} - \sum_{k=1}^{m-1}\big\{B_{j+\frac{1}{2}}^{(k)} - B_{j-\frac{1}{2}}^{(k)}\big\}\frac{(\Delta t)_k}{\Delta x} \tag{4.10}$$

with $(\Delta t)_k = \frac{(\Delta t)^{k+1}}{(k+1)!}$ and $f_{j+\frac{1}{2}}^{(0)} = f(u(x_{j+\frac{1}{2}}, 0+))$.

The solution is advanced in time by updating the cell averages according to the formula (2.3).

5. Accuracy

In this section we study the accuracy of the central ADER schemes based on flux expansion.

Firstly, with r stencils, polynomial $P_j(x)$ of degree at most $(r-1)$ can be reconstructed, and the spatial accuracy is $(2r-1)$th order in the case of the WENO interpolations:

$$P_j(x) = u\big(x, t^n\big) + o(\Delta x)^{2r-1} \tag{5.1}$$

but the spatial accuracy for the kth order derivative for u is $(r-k)$th order

$$\partial_x^{(k)} P_j(x) = u_x^{(k)}\big(x, t^n\big) + o(\Delta x)^{r-k}. \tag{5.2}$$

Also, for the function $g_j(x) = f(P_j(x))$, the following order of accuracy is estimated [8]

$$g_j(x) = f\big(x, t^n\big) + o(\Delta x)^{2r-1}, \tag{5.3}$$

$$\partial_x^{(k)} g_j(x) = f_x^{(k)}\big(x, t^n\big) + o(\Delta x)^{r-k}. \tag{5.4}$$

For the ADER method (2.3) and (3.16), the truncation error is defined by

$$T(x_j,t^n)=\frac{(u_j^{n+1}-u_j^n)}{\Delta t}+\frac{1}{\Delta x}\{F_{j+\frac{1}{2}}-F_{j-\frac{1}{2}}\}=\frac{(u_j^{n+1}-u_j^n)}{\Delta t}+\sum_{k=0}^{m-1}\frac{(\Delta t)^k}{(k+1)!}\frac{1}{\Delta x}\big[\beta_j^{(k)}(x_{j+\frac{1}{2}})-\beta_j^{(k)}(x_{j-\frac{1}{2}})\big], \tag{5.5}$$

where $\beta_j^{(k)}(x)$ are given by

$$\beta_j^{(0)}(x)=g_j(x), \tag{5.6}$$

$$\beta_j^{(k)}(x)=\beta_j^{(k)}\big(\partial_x^{(1)}g_j(x),\ldots,\partial_x^{(k)}g_j(x)\big),\quad k=1,\ldots,m-1. \tag{5.7}$$

The accuracy will be discussed on the assumption of smooth solution.

In the WENO case, the accuracy is given by

$$\beta_j^{(k)}(x)=f_t^{(k)}(x,t)+o(\Delta x)^{r-k}, \tag{5.8}$$

$$\therefore\ \frac{1}{\Delta x}\big[\beta_j^{(k)}(x_{j+\frac{1}{2}})-\beta_j^{(k)}(x_{j-\frac{1}{2}})\big]=\big(f_t^{(k)}(x,t)\big)_x+o(\Delta x)^{r-k}. \tag{5.9}$$

The time Taylor series expansion gives

$$\frac{(u_j^{n+1}-u_j^n)}{\Delta t}=\sum_{k=0}^{m-1}\frac{(\Delta t)^k}{(k+1)!}u_t^{(k+1)}(x_j,t^n)+o(\Delta t)^m. \tag{5.10}$$

Therefore, the truncation error (5.5), by using (5.8) and (5.10), takes the form

$$T(x_j,t^n)=\sum_{k=0}^{m-1}\frac{(\Delta t)^k}{(k+1)!}\big[u_t^{(k+1)}(x_j,t^n)+\big(f_t^{(k)}\big)_x\big((x_j,t^n)+o(\Delta x)^{r-k}\big)\big]+o(\Delta t)^m=\sum_{k=0}^{m-1}o\big(\Delta t^k\Delta x^{r-k}\big)+o(\Delta t)^m, \tag{5.11}$$

since from (2.1),

$$u_t^{(k+1)}(x_j,t^n)+\big(f_t^{(k+1)}\big)_x(x_j,t^n)=0. \tag{5.12}$$

If the ratio $\frac{\Delta t}{\Delta x}$ is constant, we have

$$\big|T(x_j,t^n)\big|\leqslant C_1(\Delta x)^r+C_2(\Delta t)^m. \tag{5.13}$$

By using the WENO reconstruction of order r and ADER method (3.16) of order m, we obtain the ADER scheme of order r in space and m of time. For the central ADER (4.10), in which the third order TVD flux is used, we will see the accuracy empirically.

6. Numerical experiments

In this section, we numerically study the convergence properties of the new schemes proposed here. We compare the results of these schemes with those of other state of the art high order shock capturing methods, such as WENO5 [4], third order TVD scheme [19], ADER and ADER-WAF schemes. Here we use the finite volume version of WENO5 method with third order Runge–Kutta time stepping.

The linear stability condition for the all these methods is CFL $\leqslant 1$, where CFL is the maximum Courant number for each time step; we use CFL $= 0.95$ for these methods.

In the numerical experiments we use very large output times, corresponding to hundreds of thousand time steps, with solutions consisting of both discontinuities and smooth parts.

For all tests we use a uniform mesh, N denotes the number of cells and the exact solution is shown by the solid line and the numerical solution by symbols.

We compare the following schemes:

1. ADER-r it is the rth order ADER scheme with the upwind Gudonov flux [16].
2. WENO-r it is fifth order WENO scheme with third order Runge–Kutta time stepping [16].
3. ADERr-WAF it is the rth order ADER scheme with WAF flux [16].
4. ADERr-LF it is the rth order ADER scheme with LXF flux.
5. ADERr-TVD it is the rth order ADER scheme with the third order TVD flux [19].

6.1. Accuracy tests

We first test the accuracy of the schemes on the linear scalar problems.

Table 1a
Convergence study for Eq. (6.1) with initial condition (6.2) at $t = 1$

N	EWNO5	WENO5	ADER3	ADER3	ADER3-WAF	ADER3-WAF
	L^1 error	L^1 order	L^1 error	L^1 order	L^1 error	L^1 order
10	5.99E−2		3.92E−3		2.65E−3	
20	5.52E−3	3.44	1.97E−4	4.32	1.62E−4	4.04
40	5.95E−4	3.21	2.06E−5	3.25	1.38E−5	3.55
80	7.04E−5	3.08	2.79E−6	2.89	1.55E−6	3.16
160	8.68E−6	3.02	3.56E−7	2.97	1.89E−7	3.04

Table 1b
Convergence study for Eq. (6.1) with initial condition (6.2) at $t = 1$

N	ADER3-LF	ADER3-LF	ADER3-TVD	ADER3-TVD
	L^1 error	L^1 order	L^1 error	L^1 order
10	2.05E−3		2.38E−4	
20	2.21E−4	3.21	2.04E−5	3.54
40	2.63E−5	3.08	1.24E−6	4.04
80	3.35E−6	2.97	5.38E−8	4.53
160	2.83E−7	3.13	2.66E−9	5.34

Table 1c
Convergence study for Eq. (6.1) with initial condition (6.2) at $t = 1$

N	ADER5	ADER5	ADER5-WAF	ADER5-WAF
	L^1 error	L^1 order	L^1 error	L^1 order
10	1.45E−4		1.46E−4	
20	7.84E−7	7.53	1.49E−6	6.61
40	2.52E−8	4.96	4.53E−8	5.04
80	7.73E−10	5.03	1.24E−9	5.19
160	2.34E−11	5.05	4.46E−11	4.80

Table 1d
Convergence study for Eq. (6.1) with initial condition (6.2) at $t = 1$

N	ADER5-LF	ADER5-LF	ADER5-TVD	ADER5-TVD
	L^1 error	L^1 order	L^1 error	L^1 order
10	7.37E−5		2.06E−6	
20	2.21E−6	5.06	1.98E−8	6.70
40	6.87E−8	5.00	1.96E−10	6.66
80	2.22E−9	4.95	1.88E−12	6.70
160	6.54E−11	5.09	2.11E−14	6.48

Example 1. We solve the transport equation

$$u_t + u_x = 0, \quad x \in [-1, 1], \tag{6.1}$$

subjected to periodic initial conditions

$$u(x, 0) = \sin(\pi x), \tag{6.2}$$

$$u(x, 0) = \sin^4(\pi x) \tag{6.3}$$

defined on $[-1, 1]$ and periodic boundary conditions. We use the output times are $t = 1$. Tables 1 and 2 show the convergence rates and errors in L^1 norm. We observe that ADER-r, ADERr-WAF and ADERr-LF schemes reach the designed order of accuracy while, as expected, WENO5 scheme decreases with third order only. This is due to WENO5 uses a third order Runge–Kutta time stepping. We notice that ADERr-LF schemes are comparable with ADERr-WAF schemes. The simplicity and efficiency of the central schemes, as compared with upwind schemes, should be taken into account. As expected the ADERr-TVD schemes are the most accurate in both error sizes and order of accuracy (approximately $= 4.3$ for $r = 3$ and 6.7 for $r = 5$). This is due to using a third order TVD flux instead of first order flux.

Another way of interpreting the results of Tables 1 and 2 is this: by using central, LXF flux as building block for very high order ADER methods one approaches the accuracy of the corresponding methods used with upwind fluxes based on Riemann solvers, while the use of a central third order TVD flux as a building block one obtains more accurate results. The attraction of the central, monotone and TVD, fluxes is that they are simpler, much faster and more general than a good upwind fluxes.

Table 2a
Convergence study for Eq. (6.1) with initial condition (6.3) at $t = 1$

N	EWNO5	WENO5	ADER3	ADER3	ADER3-WAF	ADER3-WAF
	L^1 error	L^1 order	L^1 error	L^1 order	L^1 error	L^1 order
10	3.68E−1		9.02E−2		9.21E−2	
20	1.20E−1	1.61	1.25E−2	2.85	8.17E−3	3.50
40	2.15E−2	2.48	1.47E−3	3.09	1.22E−3	2.75
80	2.34E−3	3.20	1.35E−4	3.44	1.20E−4	3.34
160	2.78E−4	3.08	1.42E−5	3.25	9.97E−6	3.59

Table 2b
Convergence study for Eq. (6.1) with initial condition (6.3) at $t = 1$

N	ADER3-LF	ADER3-LF	ADER3-TVD	ADER3-TVD
	L^1 error	L^1 order	L^1 error	L^1 order
10	2.39E−1		1.98E−3	
20	2.85E−2	3.07	8.97E−5	4.46
40	3.12E−3	3.19	3.62E−6	4.63
80	3.25E−4	3.26	1.58E−7	4.52
160	3.51E−5	3.15	7.41E−9	4.41

Table 2c
Convergence study for Eq. (6.1) with initial condition (6.3) at $t = 1$

N	ADER5	ADER5	ADER5-WAF	ADER5-WAF
	L^1 error	L^1 order	L^1 error	L^1 order
10	6.17E−2		6.01E−2	
20	2.84E−3	4.44	2.29E−3	4.71
40	1.35E−4	4.40	1.29E−4	4.15
80	1.02E−6	7.01	1.09E−6	6.90
160	1.32E−8	6.27	1.92E−8	5.82

Table 2d
Convergence study for Eq. (6.1) with initial condition (6.3) at $t = 1$

N	ADER5-LF	ADER5-LF	ADER5-TVD	ADER5-TVD
	L^1 error	L^1 order	L^1 error	L^1 order
10	7.69E−2		5.12E−5	
20	2.02E−3	5.25	4.25E−7	6..91
40	5.11E−5	5.30	3.65E−9	6.86
80	1.27E−7	5.32	3.71E−11	6.62
160	3.28E−8	5.28	3.98E−13	6.54

6.2. Test cases with shocks

Example 2. Now we solve (6.1) for the following initial data (see [16])

$$u(x,0) = \begin{cases} \frac{1}{6}[G(x,z-\delta) + G(x,z+\delta) + 4G(x,z)], & -0.8 \leqslant x \leqslant -0.6, \\ 1, & -0.4 \leqslant x \leqslant -0.2, \\ 1 - |10(x-0.1)|, & 0 \leqslant x \leqslant 0.2, \\ \frac{1}{6}[F(x,a-\delta) + F(x,a+\delta) + 4F(x,a)], & 0.4 \leqslant x \leqslant 0.6, \\ 0, & \text{otherwise}, \end{cases} \tag{6.4}$$

with periodic boundary condition on $[-1, 1]$.

Where $G(x,z) = \exp(-\beta(x-z)^2)$, $F(x,a) = \{\max(1-\alpha^2(x-a)^2), 0\}^{\frac{1}{2}}$.

The constants are taken as $a = 0.5$, $z = -0.7$, $\delta = 0.005$, $\alpha = 10$ and $\beta = (\log 2)/36\delta^2$.

This initial condition consists of several shapes which are difficult for numerical methods to resolve correctly. Some of these shapes are not smooth and the other are smooth but very sharp. We compute the solution at the output time $t = 20$ and very long time $t = 2000$. We use a baseline mesh of 200 cells.

Figs. 1–4 show the results of ADER3-LF, ADER3-TVD, ADER5-LF and ADER5-TVD schemes respectively at $t = 20$. Comparing the results obtained with WENO5, original ADER3, ADER5, ADER3-WAF and ADER5-WAF schemes (see [16]), the results obtained by ADERr-LF ($r = 3, 5$) are comparable with ADERr-WAF schemes and they are more accurate than WENO5 scheme

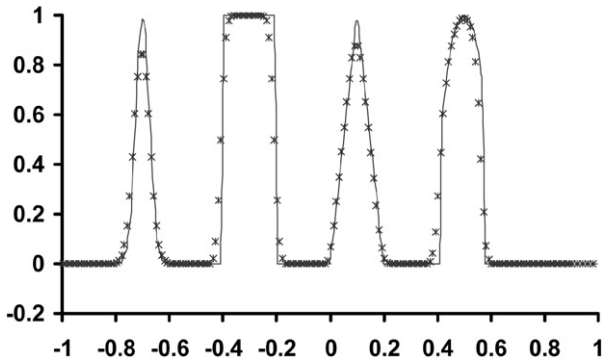

Fig. 1. Solution of Example 2 using ADER3-LF scheme at $t = 20$.

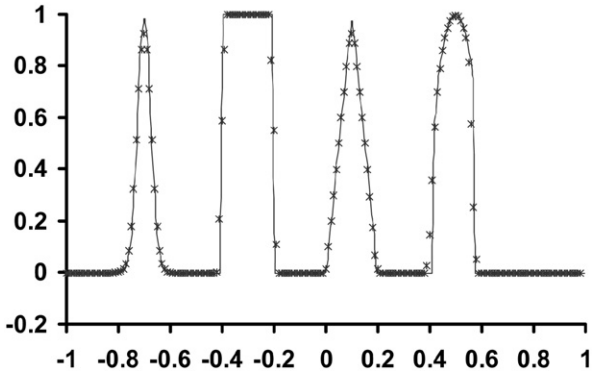

Fig. 2. Solution of Example 2 using ADER3-TVD scheme at $t = 20$.

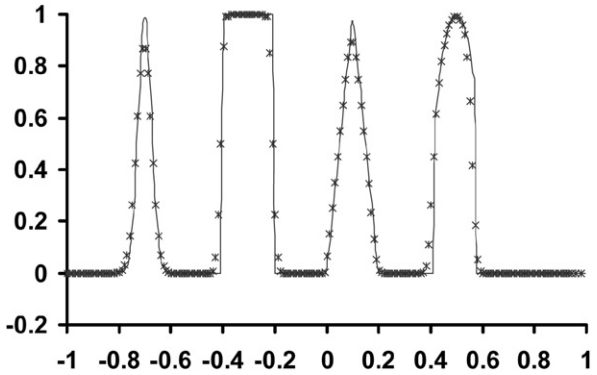

Fig. 3. Solution of Example 2 using ADER5-LF scheme at $t = 20$.

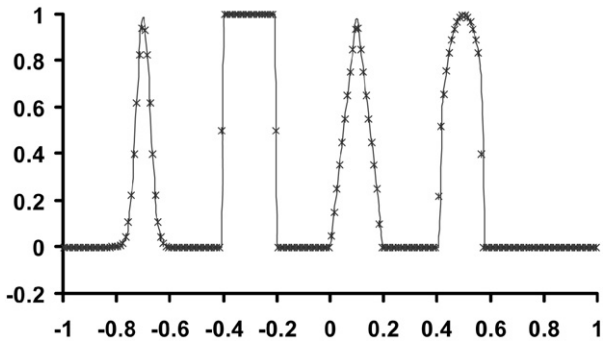

Fig. 4. Solution of Example 2 using ADER5-TVD scheme at $t = 20$.

Table 3a
Convergence study for Eq. (6.1) with initial condition (6.4) at $t = 2000$

N	EWNO5	WENO5	ADER3-WAF	ADER3-WAF	ADER4-WAF	ADER4-WAF
	L^1 error	L^1 order	L^1 error	L^1 order	L^1 error	L^1 order
200	6.73E−1		1.23E−1		4.69E−2	
400	3.82E−1	0.82	6.17E−2	0.99	2.33E−2	1.00
800	2.13E−1	0.84	3.14E−2	0.97	1.17E−2	0.99
1600	1.23E−1	0.79	1.62E−2	0.95	5.71E−3	1.03

Table 3b
Convergence study for Eq. (6.1) with initial condition (6.4) at $t = 2000$

N	ADER3-LF	ADER3-LF	ADER3-TVD	ADER3-TVD	ADER4-LF	ADER4-LF	ADER4-TVD	ADER4-TVD
	L^1 error	L^1 order	L^1 error	L^1 order	L^1 error	L^1 order	L^1 error	L^1 order
200	1.56E−1		7.96E−2		3.71E−2		4.49E−3	
400	8.33E−2	0.905	3.71E−2	1.105	1.66E−2	1.16	1.93E−3	1.22
800	4.46E−2	0.901	1.76E−2	1.072	7.88E−3	1.075	9.54E−4	1.014
1600	2.31E−2	0.955	8.44E−3	1.061	3.81E−3	1.045	4.66E−4	1.033

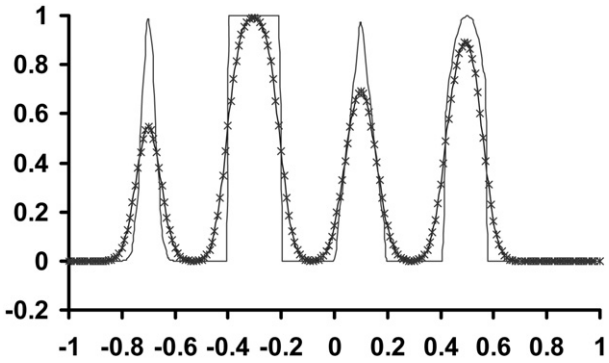

Fig. 5. Solution of Example 2 using ADER3-LF scheme at $t = 2000$.

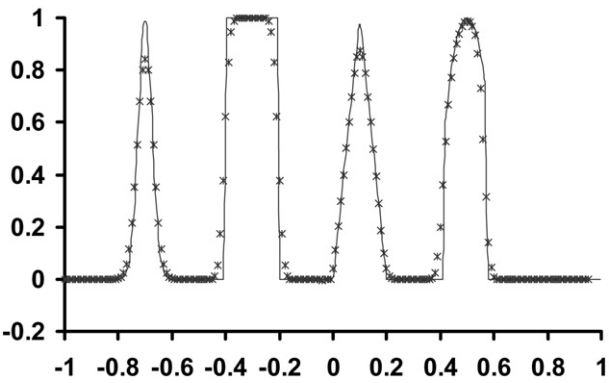

Fig. 6. Solution of Example 2 using ADER3-TVD scheme at $t = 2000$.

overall the solution. Again, we should take into account that the central schemes are simpler and faster than the upwind schemes. As expected the ADERr-TVD schemes are superior to those obtained with all the other methods.

To show the long time behaviour of the resulting schemes, Table 3 shows convergence studies for different schemes at very long time $t = 2000$. We present the errors of cell averages of the solution in L^1 norm. We observe that WENO5. ADER3-WAF, ADER4-WAF, ADER3-LF schemes achieve approximately first order of accurate as the mesh is refined while ADER3-TVD achieve approximately third order accurate. The ADER4-TVD scheme is the most accurate in both error sizes and order of accuracy. It achieves more than third order accuracy.

Figs. 5–8 depict graphical results the results of ADER3-LF, ADER3-TVD, ADER5-LF and ADER5-TVD schemes respectively, at $t = 2000$. Comparing the results in [16], we note that both ADER3 and WENO5 produce unacceptable results. They smear the square pulse into a smooth Gaussian-like wave. The ADER3-WAF and ADER5-WAF produce much more accurate results.

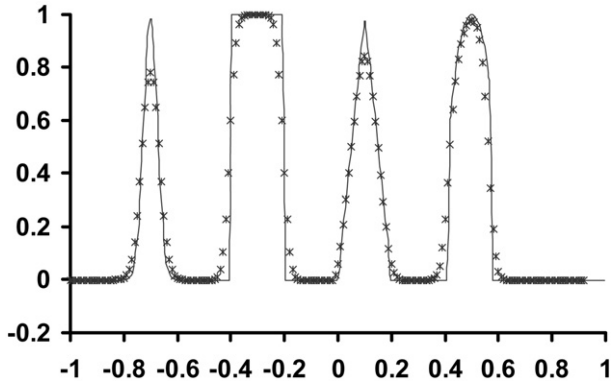

Fig. 7. Solution of Example 2 using ADER5-LF scheme at $t = 2000$.

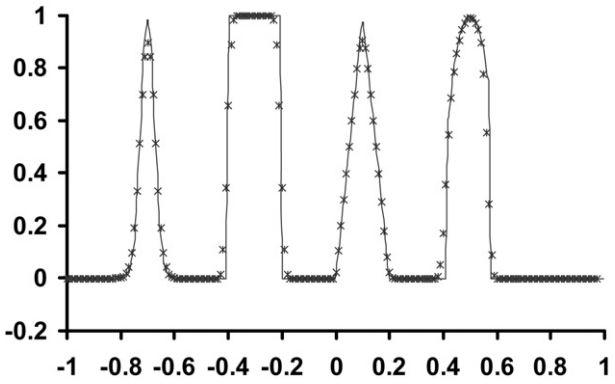

Fig. 8. Solution of Example 2 using ADER5-TVD scheme at $t = 2000$.

As expected ADER3-TVD and ADER5-TVD produce the most accurate (especially ADER5-TVD) for all parts of the solution, including the square pulse. These observations are in agreement with the convergence study in Table 3. Moreover, the results obtained with ADERr-TVD (with 200 cells) are comparable with ADERr-WAF with 400 and 1600 cells in [16] which means that the ADERr-TVD are more efficient than ADERr-WAF schemes.

6.3. Burgers' equation

Example 3. This example considers the numerical solution of the inviscid Burgers' equation

$$u_t + \left(\frac{u^2}{2}\right)_x = 0, \tag{6.5}$$

with the initial condition

$$u(x,0) = \begin{cases} -1, & |x| \geqslant 0.5, \\ 2, & |x| < 0.5. \end{cases} \tag{6.6}$$

It is well known that the Burger equation governs simple acoustic waves and hence allows shocks. In this case the jump at $x = -0.5$ creates a simple centered expansion fan with a sonic point and the jump at $x = 0.5$ creates a shock wave with speed 0.5. At $t = 2/3$ the rarefaction hits the shock and then the solution has a rarefaction wave only. The numerical solution is displayed at $t = 0.4$ (before collision of the head of the rarefaction with the shock) and $t = 1$ (after collision). Numerical results are shown in Figs. 9–11, with 80 grid points, obtained with ADER5-WAF, ADER5-LF and ADER5-TVD, respectively. We notice that ADER5-LF is still well comparable with ADER5-WAF. The simplicity and efficiency of the ADER5-LF (central) must be taken into account. Again, the ADER5-TVD is clearly superior to the other schemes.

In Table 4 we give the errors given by ADER5-WAF, ADER5-LF and ADER5-TVD at $t = 1$. We note that ADER5-TVD scheme is superior to the other schemes.

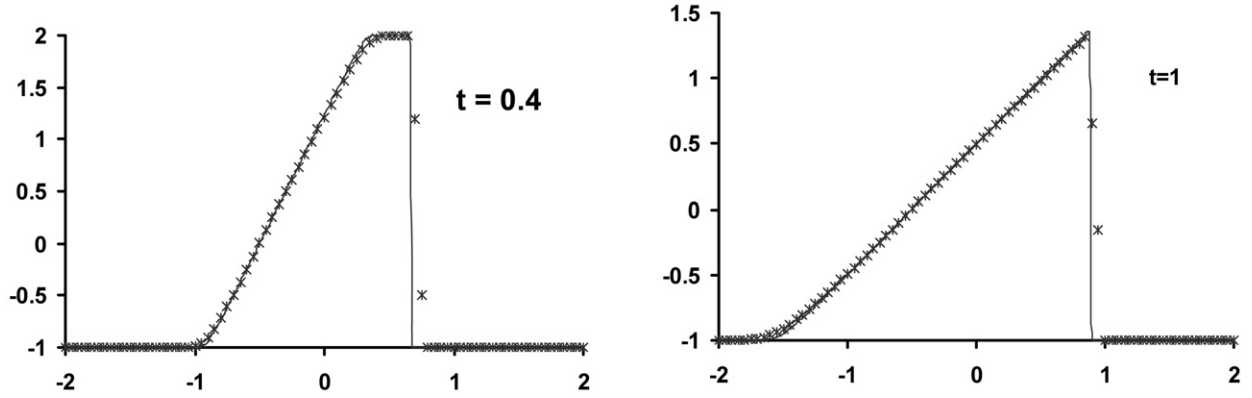

Fig. 9. Solution of Example 3 using ADER5-WAF scheme.

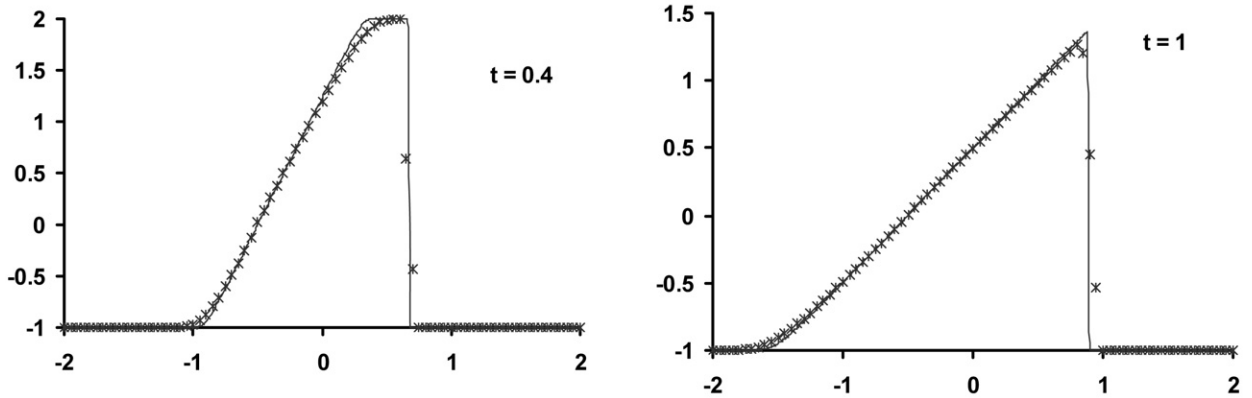

Fig. 10. Solution of Example 3 using ADER5-LF scheme.

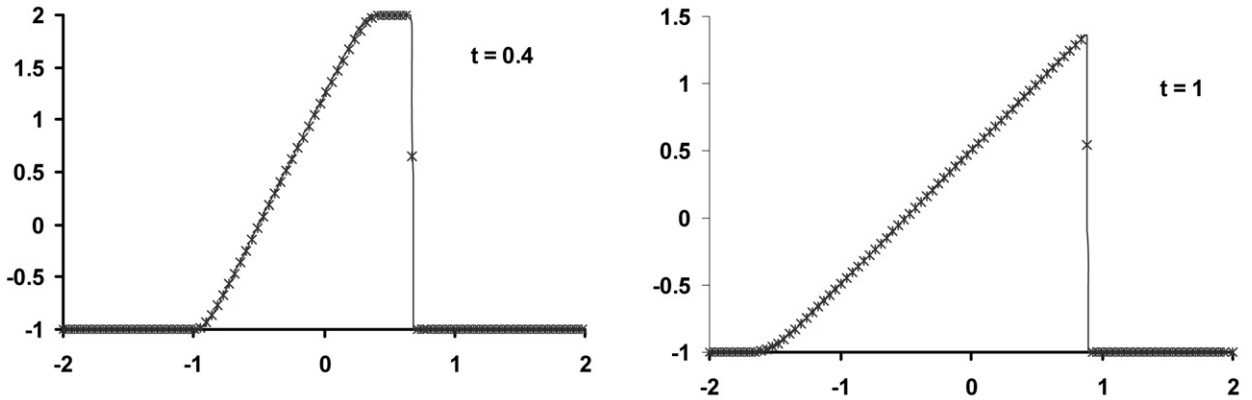

Fig. 11. Solution of Example 3 using ADER5-TVD scheme.

Table 4
Convergence study for Eq. (6.5) with initial condition (6.6) at $t = 1$

N	ADER5-WAF	ADER5-WAF	ADER5-LF	ADER5-LF	ADER5-TVD	ADER5-TVD
	L^1 error	L^1 order	L^1 error	L^1 order	L^1 error	L^1 order
20	4.42E−1		4.47E−1		4.98E−2	
40	2.13E−1	1.05	2.21E−1	1.10	2.04E−2	1.28
80	1.07E−1	1.00	9.68E−2	1.19	9.08E−3	1.17
160	5.38E−2	0.99	4.88E−2	0.99	4.19E−3	1.12

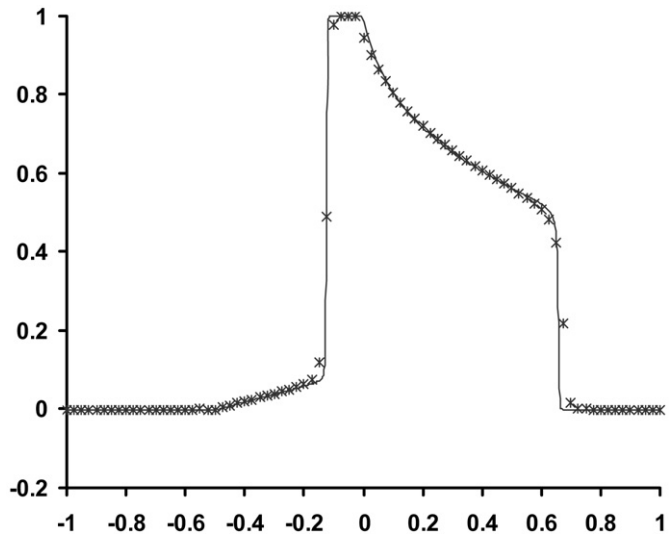

Fig. 12. Solution of Example 4 using ADER5-WAF scheme at $t = 0.4$.

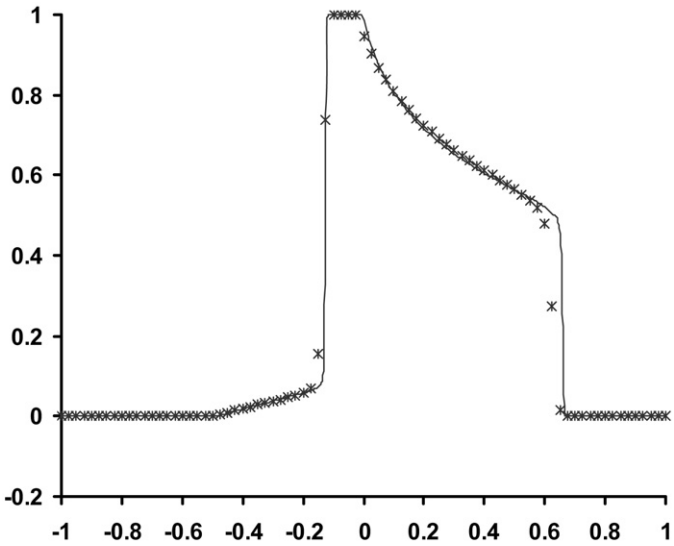

Fig. 13. Solution of Example 4 using ADER5-LF scheme at $t = 0.4$.

6.4. Buckley–Leverett equation

Example 4. The fourth test is Buckley–Leverett equation. It is a non-convex problem and is given by [6]

$$u_t + \left(\frac{4u^2}{4u^2 + (1-u)^2}\right)_x = 0, \tag{6.7a}$$

with the initial condition

$$u(x,0) = \begin{cases} 1, & -0.5 \leqslant x \leqslant 0, \\ 0, & \text{elsewhere.} \end{cases} \tag{6.7b}$$

The solution is computed at $t = 0.4$. The exact solution is a shock-rarefaction-contact discontinuity mixture. We notice that some high order schemes fail to converge to the correct entropy solution for this problem. Figs. 12–14 show the numerical results of ADER5-WAF, ADER5-LF and ADER5-TVD respectively on the mesh of 81 cells. As expected ADER5-TVD produce the most accurate for all parts of the solution while the ADER5-LF is well comparable with ADER5-WAF. Moreover, the results obtained with ADER5-TVD is more accurate than the results obtained by WENO5 and WENO9 given in [6], see Fig. 2 in [6].

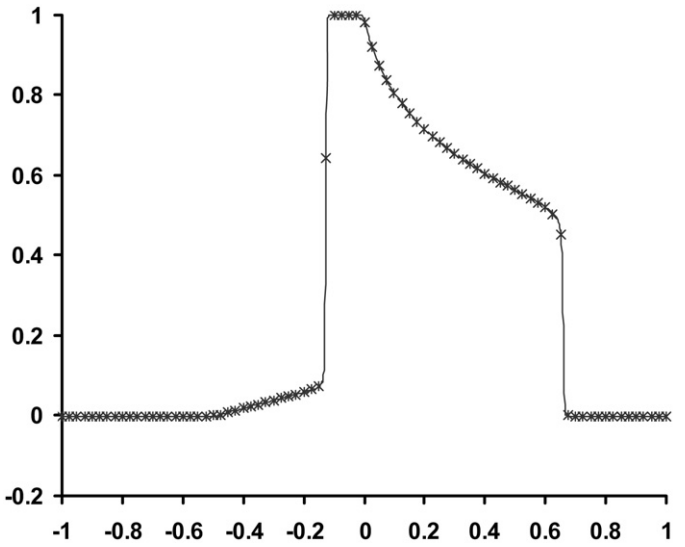

Fig. 14. Solution of Example 4 using ADER5-TVD scheme at $t = 0.4$.

Table 5
Convergence study for Eq. (6.7) at $t = 0.4$

N	ADER5-WAF	ADER5-WAF	ADER5-LF	ADER5-LF	ADER5-TVD	ADER5-TVD
	L^1 error	L^1 order	L^1 error	L^1 order	L^1 error	L^1 order
20	2.12E−1		5.27E−1		3.82E−2	
40	1.09E−1	0.96	2.38E−1	1.142	1.75E−2	1.12
80	5.26E−2	1.05	1.18E−1	1.015	8.49E−3	1.04
160	2.67E−2	0.978	5.96E−2	0.983	4.23E−3	1.005

In Table 5 we give the results at $t = 0.4$. We note that ADER5-TVD yields better accuracy than ADER5-WAF and ADER5-LF schemes.

7. Systems of conservation laws

We extend our schemes to solve hyperbolic systems of conservation laws of the form

$$U_t + F(U)_x = 0. \tag{7.1}$$

In this section we test our schemes on the system of Euler equations of gas dynamics where

$$U = (\rho, \rho u, E)^T \quad \text{and} \quad F(U) = \left(\rho u, \rho u^2 + P, u(E + P)\right)^T,$$

where ρ is the density, u is the velocity, P is the pressure, $E = 0.5\rho u^2 + \rho e$ is the total energy (sum of internal energy and kinetic energy); e is the specific internal energy $e = \frac{P}{\rho(\gamma-1)}$ and γ is the ratio of specific heats.

There are two methods to extend the numerical schemes considered, namely by doing a component-wise extension or using characteristic decomposition. In the present work, we adopt the component-wise extension which is less costly. Most central schemes fix the CFL number differently for each gas dynamics problem solved. Here we adopt a general strategy to advance in time by using an adaptive evaluation of the time step

$$\Delta t = \frac{0.95\Delta x}{\max(c_j + |u_j|)},$$

where c_j and u_j are the local sound speed and velocity, respectively. This step evaluation technique can accommodate for problems where the characteristic speed change widely in time.

7.1. Lax's problem

We solve (7.1) using the initial condition.

We solve the Lax problem [4] for Euler equations (7.1) and initial data consists of two states, left (L) and right (R)

$$(\rho_L, u_L, E_L) = (0.445, 0.311, 8.928) \quad \text{and} \quad (\rho_R, u_R, E_R) = (0.5, 0.0, 1.4275) \tag{7.2}$$

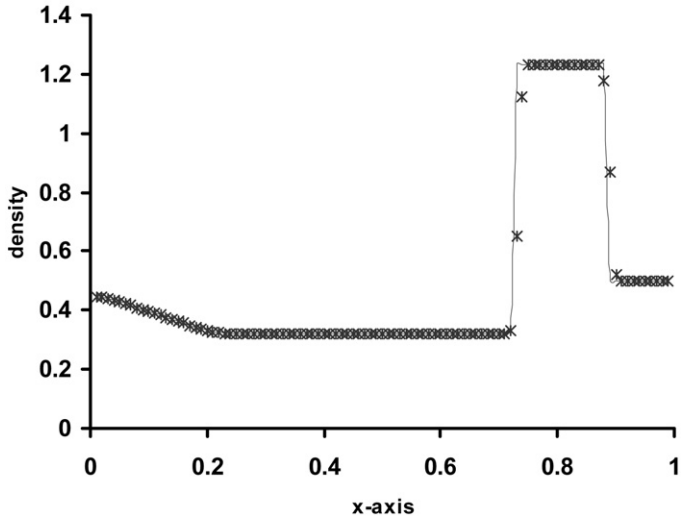

Fig. 15. Solution of Lax problem (7.2) using ADER5-WAF scheme at $t = 0.16$.

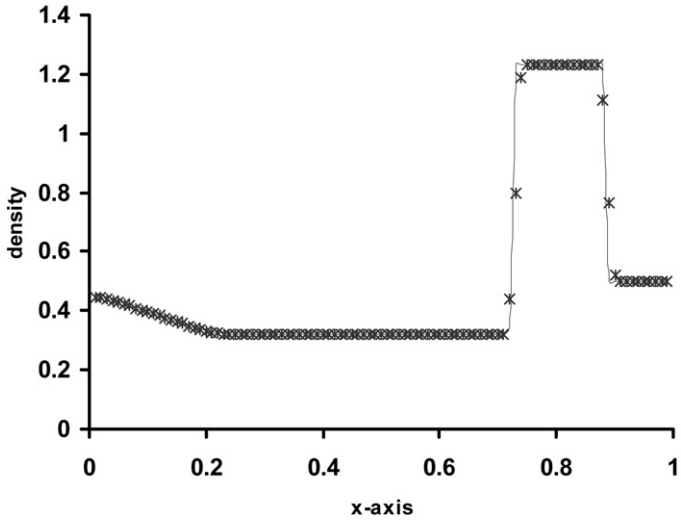

Fig. 16. Solution of Lax problem (7.2) using ADER5-LF scheme at $t = 0.16$.

separated by a discontinuity at $x = 0.5$. The computational domain is taken as the unit interval $[0, 1]$. Figs. 15–17 show the performance of ADER5-WAF, ADER5-LF and ADER5-TVD respectively at $t = 0.16$ with 100 cells. Comparing the results in Figs. 15–17 we note that the ADER5-TVD scheme is still better than the other schemes.

7.2. Blast wave problem

The blast problem introduced by Woodward and Colella [18] is severe test problem and therefore a good problem to test the robustness of numerical schemes. This problem has the initial condition consists of three states

$$U(x,0) = \begin{cases} (\rho_L, u_L, P_L) = (1, 0, 1000), & x < 0.1, \\ (\rho_M, u_M, P_M) = (1, 0, 0.01), & 0.1 < x < 0.9, \\ (\rho_R, u_R, P_R) = (1, 0, 100), & x > 0.9, \end{cases} \tag{7.3}$$

with $\gamma = 1.4$. Boundary conditions are reflective. The solution of this problem contains the propagation of strong shock waves into low pressure regions, the collision of strong shock waves and interaction of shock waves and rarefactions, and is thus a good test of the schemes.

We display the numerical results of the density and velocity of this complex problem in Fig. 18. The results are with 200 cells at time $t = 0.28$ and $t = 0.38$ and we get the exact solution from WENO [4] scheme on 4000 cells.

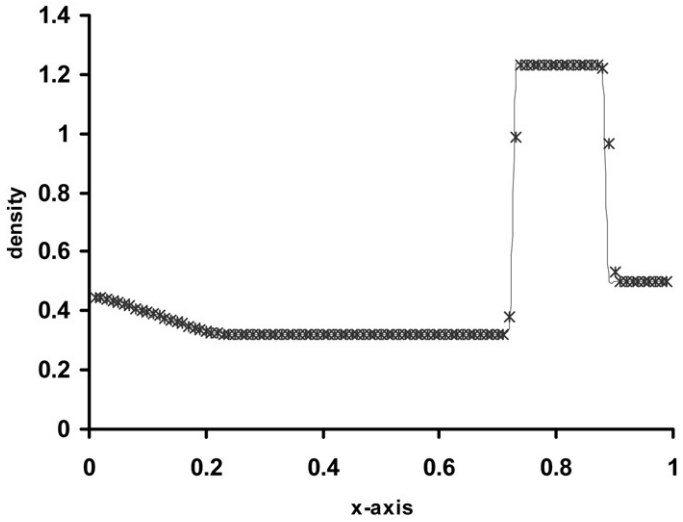

Fig. 17. Solution of Lax problem (7.2) using ADER5-TVD scheme at $t = 0.16$.

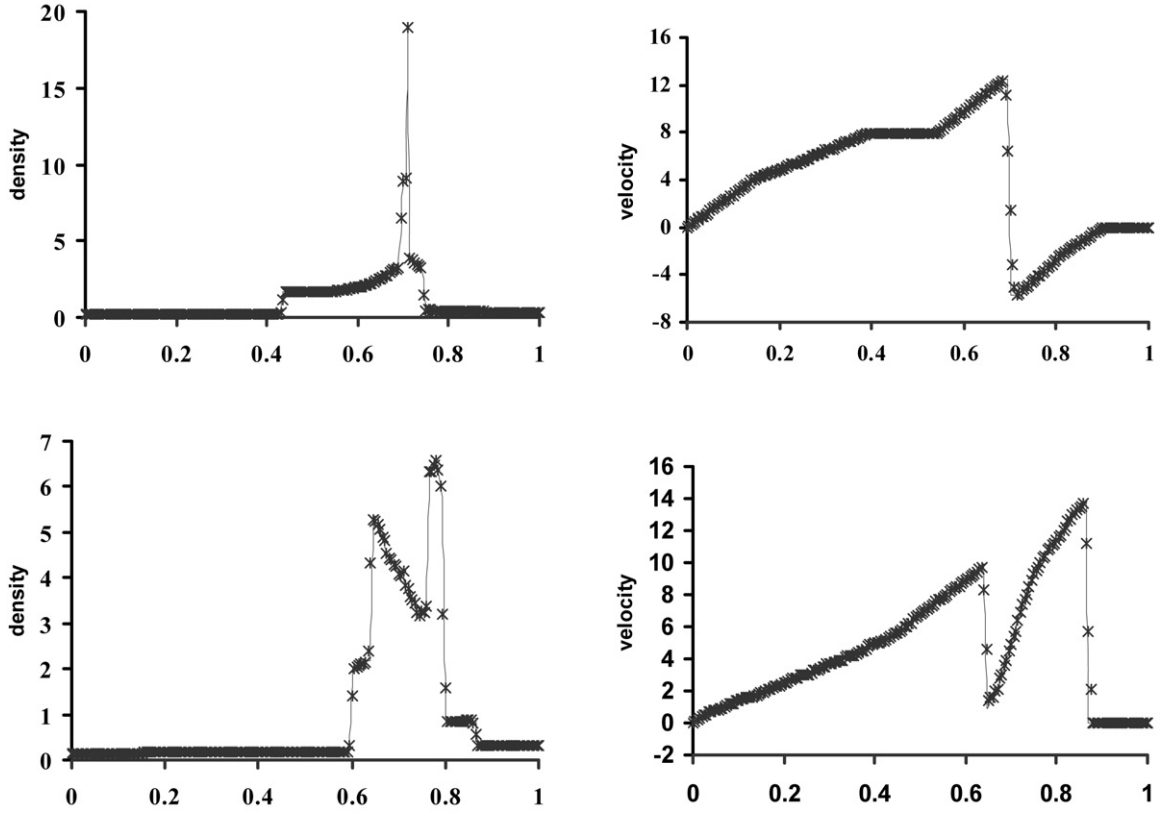

Fig. 18. Velocity and density of blast problem (7.3) using ADER5-TVD at $t = 0.028$ (up) and $t = 0.038$ (down).

Fig. 18 shows the density and velocity obtained by ADER5-TVD scheme It is noticed that the ADER5-TVD scheme is able to obtain such sharp resolution of the complex double blast problem, particularly, the density peaks have almost the correct value.

7.3. Shock/turbulence interaction problem

To show the advantages of our scheme, we will solve a problem with a rich smooth structure and a shock wave. A typical example for this is the problem of shock interaction with entropy waves.

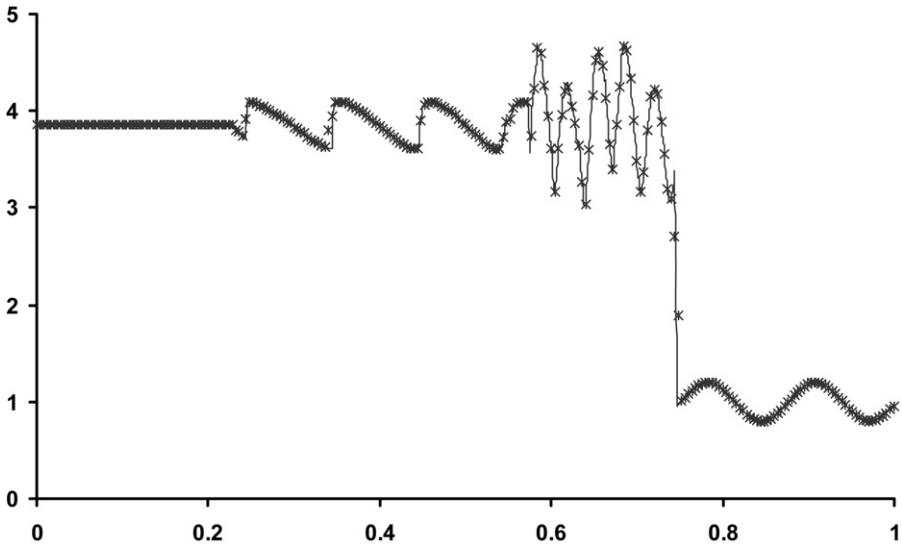

Fig. 19. Density of problem (7.4) using ADER5-WAF method.

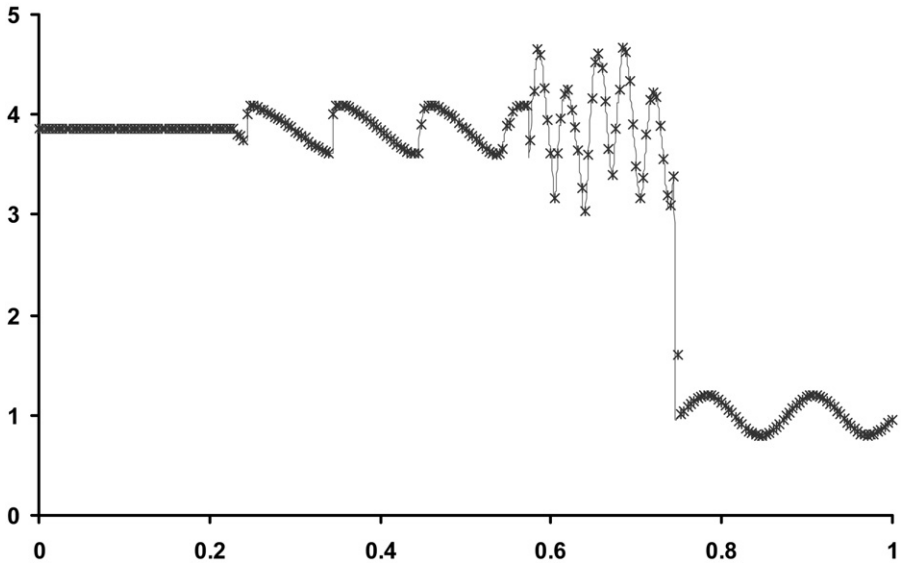

Fig. 20. Density of problem (7.4) using ADER5-TVD method.

We solve the Euler equations (7.1) with a moving Mach = 3 shock interacting with sine waves in density; i.e., initially

$$(\rho_L, u_L, P_L) = (3.857143, 2.629369, 10.3333), \quad \text{for } x \leqslant 0.1,$$
$$(\rho_R, u_R, P_R) = (1 + 0.2\sin 50x, 0, 1), \quad \text{for } x > 0.1. \tag{7.4}$$

The flow contains physical oscillations which have to be resolved by the numerical method. We compute the solution at $t = 0.18$. Figs. 19 and 20 show the computed density by ADER5-WAF and ADER5-TVD schemes against the reference solution, which is a converged solution computed by the fifth order finite difference WENO scheme [4] with 2000 grid points. Here we use 200 grid points.

We observe that ADER5-TVD scheme produces the most accurate, which is very close to the reference solution and is less expensive.

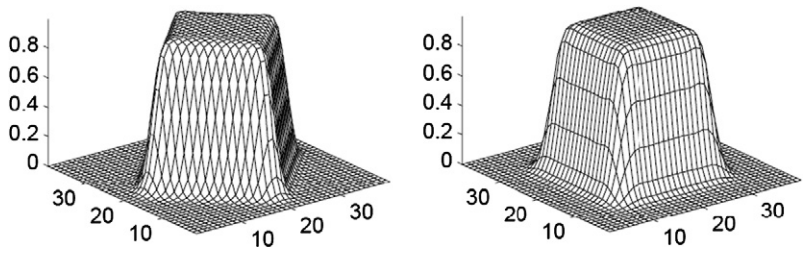

Fig. 21. Solution of (8.3) at $t = 0.5$ (left) and $t = 1.0$ (right) using ADER5-TVD scheme.

8. Extension to multidimensional problems

The present schemes can be applied to multidimensional problems by means of space operator splitting. As an example we consider the two-dimensional, Euler equations

$$U_t + \big[F(U)\big]_x + \big[G(U)\big]_y = 0. \tag{8.1}$$

There are several versions of space splitting. Here we take the simplest one, whereby the two-dimensional problem (8.1) is replaced by the sequence of two one-dimensional problems

$$U_t + \big[F(U)\big]_x = 0, \tag{8.2a}$$

$$U_t + \big[G(U)\big]_y = 0. \tag{8.2b}$$

If the data U^n at time level n for problem (8.1) are given, the solution U^{n+1} at time level $n+1$ is obtained in the following two steps:

(a) solve Eq. (8.2a) with data U^n to obtain an intermediate solution $\bar{U}^{n+1}$ (x-sweep);
(b) solve Eq. (8.2b) with data $\bar{U}^{n+1}$ to obtain the complete solution U^{n+1} (y-sweep).

For three-dimensional problems there is an extra z-sweep.

8.1. Linear equation in two dimensions

Firstly we solve the linear advection problem

$$u_t + u_x + u_y = 0 \tag{8.3a}$$

we consider the linear rotation of a square patch on $(0, 1)^2$, with initial condition

$$u_0(x, y) = \begin{cases} 1, & |x - 0.5| < 0.5,\ |y - 0.5| < 0.5, \\ 0, & \text{otherwise}, \end{cases} \qquad (x, y) \in [0, 1] \times [0, 1]. \tag{8.3b}$$

Fig. 21 shows the solution at $t = 0.5$ and $t = 1$ using ADER5-TVD scheme after a rotation of $\pi/4$ and $\pi/2$. The solution is completely free of spurious oscillations and is well.

8.2. Double Mach reflection problem

Here we solve Eq. (8.1) with

$$U = (\rho, \rho u, \rho v, E)^T, \qquad F(U) = \big(\rho u, P + \rho u^2, \rho uv, u(P + E)\big)^T, \qquad G(U) = \big(\rho v, \rho uv, P + \rho v^2, v(P + E)\big)^T.$$

The governing equation for this problem is the two-dimensional Euler equations (8.1). The computational domain of interest is a region of 4 units long and 1 unit wide. At the initial time $t = 0$ a right-moving shock wave of shock Mach number equal to 10 is set up. The reflecting wall lies at the bottom of the computational domain starting from $x = \frac{1}{6}$. Initially a right-moving shock is positioned at $(x, y) = (\frac{1}{6}, 0)$ and makes 60° angle with the x-axis. For the bottom boundary, the exact post-shock condition is imposed from $x = 0$ to $x = \frac{1}{6}$ and a reflective boundary condition is used for the rest of the x-axis. At the top boundary of the computational domain, the data is set to describe the exact motion of the Mach 10 shock; consult [18] for a detailed discussion of this problem. The solution is studied for the output time $t = 0.2$.

Figs. 22 and 23 show the computed density by ADER5-WAF and ADER5-TVD schemes on the 960×240 cells. We observe that all the schemes produce the flow pattern generally accepted in the present literature [18] as correct. All discontinuities are well resolved and correctly positioned. Comparing ADER5-WAF and ADER5-TVD schemes we observe that the numerical results of the ADER5-TVD scheme are better and also we notice that the ADER5-TVD scheme is more efficient.

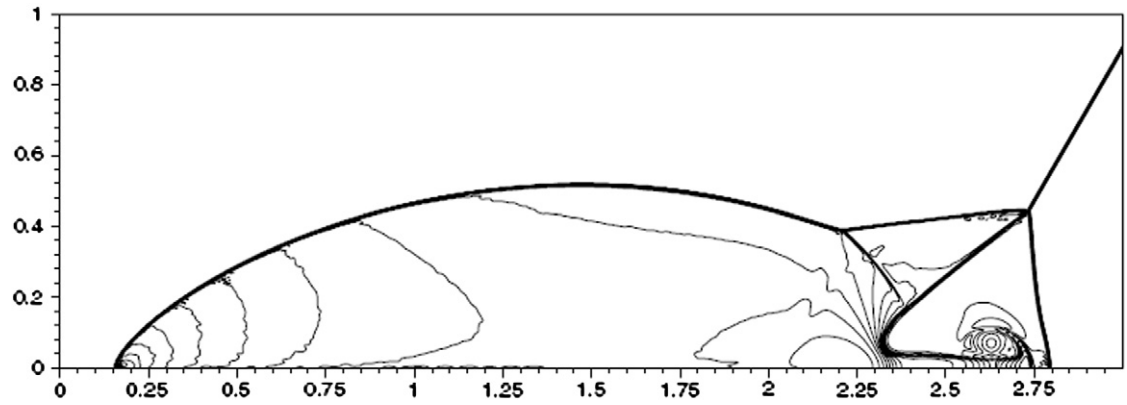

Fig. 22. Density of the double Mach reflection problem using ADER5-WAF scheme. Meshes: 960 × 240 cells. 30 contour lines from 2 to 22.

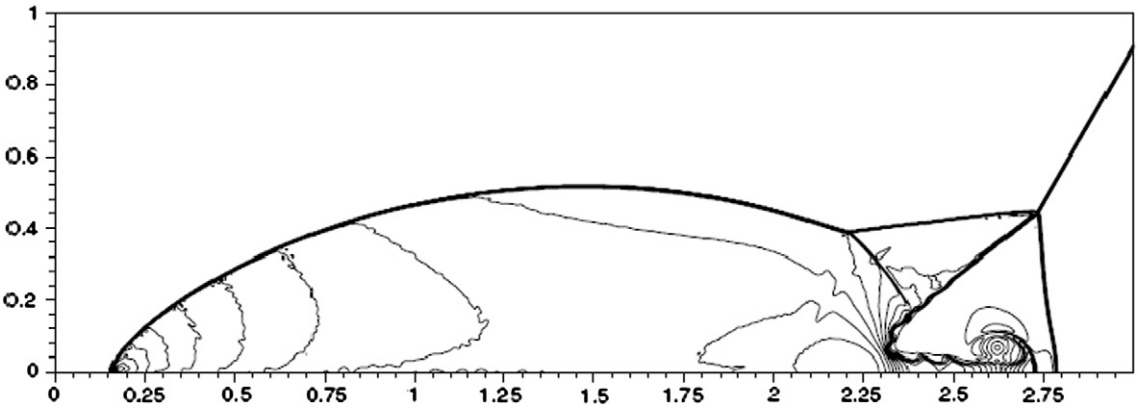

Fig. 23. Density of the double Mach reflection problem using ADER5-TVD scheme. Meshes: 960 × 240 cells. 30 contour lines from 2 to 22.

References

[1] D.S. Balsara, C.-W. Shu, Monotonicity preserving weighted essentially non-oscillatory schemes with increasingly high order of accuracy, J. Comput. Phys. 160 (2000) 405–452.
[2] A. Harten, High resolution schemes for hyperbolic conservation laws, J. Comput. Phys. 49 (1983) 357–393.
[3] A. Harten, B. Engquist, S. Osher, S. Chakravarthy, Uniformly high order accurate essentially non-oscillatory schemes III, J. Comput. Phys. 71 (1987) 231–303.
[4] G.S. Jiang, C.W. Shu, Efficient implementation of weighted ENO schemes, J. Comput. Phys. 126 (1996) 202–228.
[5] H. Nessyahu, E. Tadmor, Non-oscillatory differencing for hyperbolic conservation laws, J. Comput. Phys. 87 (1990) 408–463.
[6] J. Qiu, C.-W. Shu, On the construction, comparison, and local characteristic decomposition for the high order central WENO schemes, J. Comput. Phys. 183 (2002) 187–209.
[7] J. Shi, E.F. Toro, Fully discrete high resolution schemes for hyperbolic conservation laws, Internat. J. Numer. Methods Fluids 23 (1996) 241–269.
[8] Y. Takakura, Direct expansion forms of ADER schemes for conservation laws and their verification, J. Comput. Phys. 219 (2006) 855–878.
[9] V.A. Titarev, E.F. Toro, ADER: Arbitrary high order Godunov approach, J. Sci. Comput. 17 (2002) 609–618.
[10] V.A. Titarev, E.F. Toro, High order ADER schemes for scalar advection–diffusion–reaction equations, Int. J. Comput. Fluid Dyn. 12 (2003) 1–6.
[11] V.A. Titarev, E.F. Toro, ADER schemes for three-dimensional nonlinear hyperbolic systems, J. Comput. Phys. 204 (2005) 715–736.
[12] V.A. Titarev, E.F. Toro, Analysis of ADER and ADER-WAF schemes, IMA J. Numer. Anal. 27 (2007) 616–630.
[13] E.F. Toro, A weighted average flux method for hyperbolic conservation laws, Proc. R. Soc. Lond. Ser. A 423 (1989) 401–418.
[14] E.F. Toro, R.C. Millington, L.A.M. Nejad, Towards very high order Godunov schemes, in: E.F. Toro (Ed.), Godunov Methods: Theory and Applications, Kluwer/Plenum Academic Publishers, 2001, pp. 907–940.
[15] E.F. Toro, V.A. Titarev, Solution of the generalised Riemann for advection–reaction equations, Proc. R. Soc. Lond. 458 (2018) (2002) 271–281.
[16] E.F. Toro, V.A. Titarev, TVD fluxes for the high-order ADER schemes, J. Sci. Comput. 24 (3) (2005) 285–309.
[17] E.F. Toro, V.A. Titarev, Derivative Riemann solvers for systems of conservation laws an ADER methods, J. Comput. Phys. 212 (2006) 150–165.
[18] P. Woodward, P. Colella, The numerical solution of two dimensional fluid flow with strong waves, J. Comput. Phys. 54 (1984) 115–173.
[19] Yousef H. Zahran, Third order TVD scheme for hyperbolic conservation laws, Bull. Belg. Math. Soc. Simon Stevin 14 (2007) 259–275.